One-dimensional airflow in unsaturated zone induced by periodic water table fluctuation

Hailong Li[1]

School of Environmental Studies, China University of Geosciences, Wuhan, China

Jiu Jimmy Jiao

Department of Earth Sciences, University of Hong Kong, Hong Kong, China

Received 21 December 2004; revised 15 January 2005; accepted 1 February 2005; published 12 April 2005.

[1] This paper investigates the vertical airflow driven by fluctuating water table within the lower layer of a coastal two-layered system. The upper layer is unsaturated and semipermeable, while the lower is permeable. An analytical solution of the subsurface air pressure fluctuation is derived on the basis of model simplification assumptions, the reasonability of which was examined by numerical solutions of the original nonlinear model. The airflow in the upper layer is controlled from the top by the constant atmospheric pressure and from the bottom by a temporally fluctuating air pressure $P_0(t)$, which is spatially constant in the unsaturated zone of the lower layer. For a sinusoidal head the amplitude of $P_0(t)$ increases with the frequency of the head fluctuation, the upper layer's thickness, and the unconfined aquifer's air-filled porosity and decreases with the upper layer's permeability. The phase shift of $P_0(t)$ ranges from 0 to $\pi/2$, indicating a "time advance." Particularly, $P_0(t)$ is approximately proportional to the temporal derivative of the head for sufficiently thin or permeable upper layer and to the head itself for sufficiently thick or less permeable one. The fluctuation amplitude of the water table is always less than that of the head and can be only one tenth of the latter if the upper layer is sufficiently thick or less permeable, which may slow significantly the landward attenuation speed of the tide-induced head fluctuation in a coastal "air-confined" aquifer. The analytical solution was used to estimate the value range of the air permeability of the marine sand fill at a coastal reclamation area of Hong Kong.

Citation: Li, H., and J. J. Jiao (2005), One-dimensional airflow in unsaturated zone induced by periodic water table fluctuation, *Water Resour. Res.*, *41*, W04007, doi:10.1029/2004WR003916.

1. Introduction

[2] Airflow in unsaturated soils is of great importance in various fields such as agricultural, nuclear, environmental engineering [*Shan*, 1995; *Moridis and Pruess*, 1995; *Elberling et al.*, 1998] and has been studied for nearly one century. The study of airflow in unsaturated zone has become more attractive to researchers in the last decades. Various analytical solutions have been derived to simulate airflow problems such as one-dimensional radial [e.g., *Massmann* 1989 ; *McWhorter*, 1990] or layered [*Shan*, 1995], and two-dimensional axisymmetrical [*Baehr and Hult*, 1991; *Shan et al.*, 1992]. *Shan et al.* [1999] considered airflow in the faulted zone (one-dimensional) and the surrounding rock matrix (two-dimensional). The single-well radial solution is also applied to multiwell system using the superposition principle [*Ross and Lu*, 1994]. *Illman and Neuman* [2000] discussed the linearization of airflow equations and derived analytical solutions of radial and spherical flow from wells. *Illman and Neuman* [2001] considered the airflow to well in a fully three-dimensional unsaturated zone.

[3] In coastal areas, the water table fluctuates in response to the sea tide and the fluctuation can be decomposed into sinusoidal components [*Nielsen*, 1990; *Li and Barry*, 2000]. Sinusoidal fluctuating water level was also used in laboratory to investigate water table dynamics under capillary fringes [*Nielsen and Perrochet*, 2000]. Air pressure in coastal unsaturated zones fluctuates with sea tides, as does the groundwater level in the aquifers. Under some circumstances, the pressure can be so great that dome-shaped heave features have been observed in areally extensive paved coastal areas of Hong Kong [*GCG* (Asia), 2001]. In addition to its engineering implications, the constant air exchange in the ecologically active intertidal areas induced by seawater fluctuation may have some biological effects on the coastal plants and organisms because such an exchange will enhance the ventilation of oxygen and transport of nutrients [*Jiao and Li*, 2004]. Although tide-induced groundwater flow in saturated aquifers has been widely investigated, air pressure fluctuations in unsaturated zones have not been well addressed in the literature.

[4] Recently, *Jiao and Li* [2004] initiated investigations on subsurface airflow induced by fluctuating water table in the coastal areas. To understand the abnormally high air

[1] Also at Department of Mathematics, Anshan Normal University, Anshan, China.

0043-1397/05/2004WR003916$09.00

pressure under asphalt pavements in a coastal area in Hong Kong, a falling-pressure method was introduced to measure air permeability of asphalt in laboratory [*Li et al.*, 2004], a two-dimensional cross-section numerical model was used to simulate the air pressure fluctuations beneath asphalt ways caused by the sea tide [*Jiao and Li*, 2004]. Their numerical model shows that, for this case, the problem could be approximated as a one-dimensional vertical airflow problem with the tidal water table variation providing the piston effect.

[5] To the best knowledge of the authors, there has been no analytical study on the airflow driven by the fluctuating water table. The aim of this paper is to develop a quick analytical solution to understand the relation among the air pressure, water table fluctuation, aquifer structure and air permeability of the layers under some assumptions. The analytical solution considers a two-layered air-water subsurface system, which is common in Hong Kong where reclaimed coastal areas are paved by low-permeability surface. An unconfined coastal aquifer lies in the lower permeable layer which is overlain by a semipermeable unsaturated layer. On the basis of suitable assumptions and approximations, the original nonlinear model of air-water two-phase flow in the two layers is simplified into a linear single-phase model in the upper layer. The reasonability and reliability of the assumptions and approximations were examined by comparison of the analytical solution with the numerical solution of the original nonlinear model. Because of the air pressure fluctuation, the local water table differs significantly from the local hydraulic head in a piezometer screened at the bottom of the lower layer. An important parameter called air-leaking resistance is introduced to describe the impact of the upper semipermeable layer on the airflow. It is found that the airflow can influence significantly the tide-induced water table fluctuation of a coastal unconfined aquifer if it is overlain by low-permeability material. The analytical solution was used to estimate the value range of the air permeability of the marine sand fill at a coastal reclamation area of Hong Kong.

2. Mathematical Models for Tide-Induced Airflow

2.1. Model Description for Numerical Simulation

[6] Consider an air-water system in a coastal area composed of two horizontal layers. The upper layer lies in the unsaturated zone. The lower layer forms an unconfined aquifer which abuts a tidal water body. The water table of the unconfined aquifer, which fluctuates within the lower layer in response to the tidal level fluctuations, forms the lower boundary of the system and causes airflow therein. When the water table increases, it expels the pore air so that the ground surface exhales. When the water table decreases, it leaves extra pore space for the pore air so that the ground surface inhales. Assume that (1) the subsurface system is in an isothermal condition at 25°C, (2) the water and air are immiscible, the vaporized water in the air and the dissolution of air by the water are negligible, (3) there are no sinks or sources, and (4) the airflow in the unsaturated zone induced by the water table fluctuation is one-dimensional (vertical). Horizontal airflow can be neglected.

[7] At room temperature, assumption 2 is reasonable because the air dissolves into water at most by about 1.5% by volume [*Weir and Kissling*, 1992] and the water vaporization is very slow. In reality, the water table fluctuates with different amplitudes and phase shifts at different locations. Therefore the airflow driven by the fluctuating water table is not strictly vertical. However, if the depth of the water table is small enough and the attenuation of the water table fluctuation is not significant, the airflow driven by the fluctuating water table can be approximately regarded as vertical flow.

[8] Let the z axis be vertical, positive upward with the origin at the ground surface. The respective thickness of the lower and upper layer is b_L and b_U. Let $W(t)$ be the water table of the unconfined aquifer, i.e., the real elevation of the air-water interface of the unconfined aquifer, and $H_P(t)$ be the hydraulic head of the unconfined aquifer measured in a piezometer screened only at the bottom of the lower layer. The tide-induced local fluctuation of the head of the unconfined aquifer at a fixed inland location can be usually expressed as [e.g., *Nielsen* 1990]

$$H_P(t) = -D + \sum_{i=1}^{N} A_i \cos(\omega_i t + c_i), \tag{1}$$

where D is the distance from the surface to the mean head (see Figure 1), N is the number of sinusoidal components of the tide-induced local head fluctuation, A_i, ω_i and c_i are the amplitude, frequency and phase shift of the ith component, respectively.

[9] When the water table rises, the air pressure $P^a(z,t)|_{z=W(t)}$ in the pores immediately above the water table will be higher than the atmosphere pressure, in this case $W(t)$ will be lower than $H_P(t)$ (see Figure 1). When the water table falls, the process is reversed and $W(t)$ will be higher than $H_P(t)$. The water table $W(t)$ is unknown because it is related to the unknown air pressure $P^a(z,t)|_{z=W(t)}$.

[10] Under the assumptions 1–4, the above one-dimensional air-water two-phase flow system can be simulated using TOUGH2 numerical simulator [*Pruess et al.*, 1999]. In the TOUGH2, the air pressure P^a and the degree of gas saturation S^a are chosen to be the primary variables. The nonlinear governing equations of the air-water two-phase flow are given by *Pruess et al.* [1999] and will not given here. As far as the boundary conditions are concerned, the air pressure P^a equals the atmospheric pressure P_{atm} on the surface and $P_{atm} + \rho^w g H_P(t)$ at the bottom of the lower layer. Here ρ^w is the water density [ML^{-3}], g is the gravitational acceleration [LT^{-2}]. The gas saturation S^a equals 0 at the bottom of the lower layer and the ratio of the effective to the total air-filled porosity of the upper layer on the soil surface.

[11] The air pressure in the unsaturated zone is usually affected significantly by barometric pressure fluctuations, but not always so, e.g., in the coastal area considered by *Jiao and Li* [2004] the water table fluctuation dominates the air flow. During the 72-hour period from 7 to 9 February 2001 the amplitude of the daily fluctuation of the barometric pressure is only about 0.5 kPa, but the amplitude of the daily fluctuation of the air pressure observed in the subsoil, which is mainly induced by the water table fluctuation, is as much as 2.5 kPa [see *Jiao and Li*, 2004, Figure 2a]. Our numerical simulation based on TOUGH2 simulator also

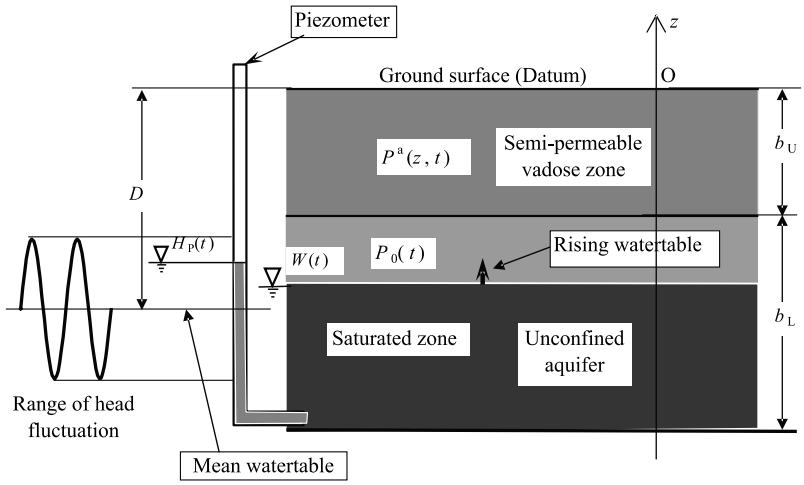

Figure 1. Schematic of airflow induced by fluctuating water table.

indicated that the barometric pressure fluctuation can be considered in a very simple way just by subtracting the barometric fluctuation data from the subsoil air pressure without loss of much accuracy. On the basis of this reason, in this paper the atmospheric pressure P_{atm} is assumed to be a constant.

[12] The initial conditions of P^a and S^a are replaced by the periodicity of P^a and S^a: $P^a(z, t) = P^a(z, t + t_P)$, $S^a = S^a(z, t + t_P)$, where t_P is the period of the periodic function (1). The definition of t_P is given by *Li and Jiao* [2003, equation (9c)]. However, for numerical solutions a hypothetical initial condition is necessary. To obtain periodic numerical solutions, the simulations were run for sufficiently large number ($5 \sim 20$) of tidal cycles until the effects of the initial conditions become negligible and the numerical solution becomes periodical. The results were then recorded and analyzed.

2.2. Simplified Model for Analytical Solution

[13] In order to obtain the analytical solutions, the nonlinear air-water two-phase flow model has to be simplified using some extra assumptions. These assumptions are the gravitational effect of air phase is negligible (assumption 5); the lower layer is so permeable that the spatial variation of the air pressure $P^a(z, t)$ within the range $W(t) \le z \le -b_U$ is negligible, the air pressure therein only depends on time and can be defined by $P_0(t)$ (assumption 6); the lower layer is so permeable that the vertical hydraulic gradient of the unconfined aquifer is negligible, the head at different depth is therefore equal to $H_P(t)$ (assumption 7); the capillary effects in the lower layer is negligible (assumption 8). With these assumptions, the study domain is restricted within the upper layer ($-b_U < z < 0$) with a new unknown $P_0(t)$. The reasonability of these assumptions will be examined by numerical solutions in section 3.2. If the variation range of P^a is less than one tenth of the atmospheric pressure P_{atm}, based on the ideal gas law, the governing equation for air in the upper layer can be linearized as [e.g., *Shan*, 1995]

$$\frac{n_{aU}\mu^a}{P_{atm}k_U}\frac{\partial P^a}{\partial t} = \frac{\partial^2 P^a}{\partial z^2}, \qquad -b_U < z < 0, \tag{2a}$$

where n_{aU} is air-filled effective porosity of the upper layer (see Figure 1), μ^a is the viscosity [$ML^{-1}\,T^{-1}$] of air, k_U is the air permeability [L^2] of the upper layer. The boundary condition at the ground surface is

$$P^a(z,t)|_{z=0} = P_{atm}. \tag{2b}$$

In order to derive the boundary conditions at the bottom of the upper layer, consider $q(-b_U, t)$, the vertical isothermal volumetric flux [LT^{-1}] of air through the soil cross section at $z = -b_U$. According to the extended Darcy's law for gases [*Stonestrom and Rubin*, 1989], one has

$$q(z,t)|_{z=-b_U} = -\frac{k_U}{\mu^a}\lim_{z\downarrow -b_U}\frac{\partial P^a}{\partial z}. \tag{3a}$$

[14] Because of pressure balance and assumptions 6–8, the head $H_P(t)$ and the water table $W(t)$ of the unconfined aquifer satisfy (see Figure 1)

$$W(t) + \frac{P_0(t)}{\rho^w g} = H_P(t) + \frac{P_{atm}}{\rho^w g}. \tag{3b}$$

Consider a vertical column within the range $W(t) \le z \le -b_U$ and with unit horizontal cross-section area. According to the mass conservation law, the initial air mass M_0 in the vertical column at initial time $t = 0$ equals the sum of the air mass contained in the layer at time t and the air mass through the bottom $z = -b_U$ during the period [0, t], i.e.,

$$M_0 = n_{aL}[-b_U - W(t)]\rho^a(z,t)|_{z=-b_U} + \int_0^t [q(z,\tau)\rho^a(z,\tau)]|_{z=-b_U}d\tau, \tag{3c}$$

where n_{aL} is the air-filled effective porosity of the lower layer (see Figure 1), ρ^a is the air density [ML^{-3}]. The second term represents the air mass through the upper layer's bottom during the period [0, t] (positive for mass loss and negative for mass gain). Differentiating equation (3c) with respect to time, substituting the expression of $W(t)$ obtained from (3b) into the resultant equation, then using the ideal gas law, and substituting (3a) and (1) into the resultant equation, yield

$$\lim_{z\downarrow -b_U}\frac{\partial P^a}{\partial t} = \frac{dP_0}{dt} = -\frac{\rho^w g}{\xi(t)}\sum_{i=1}^{N} A_i\omega_i\sin(\omega_i t + c_i) + \frac{k_U\rho^w g}{\xi(t)\mu^a n_{aL}}\lim_{z\downarrow -b_U}\frac{\partial P^a}{\partial z}, \tag{3d}$$

where

$$\xi(t) = 2 + \frac{1}{P_0(t)}\left[\rho^w g\left(-b_U + D - \sum_{i=1}^{N} A_i \cos(\omega_i t + c_i)\right) - P_{atm}\right]. \quad (3e)$$

Equation (3d) is the boundary condition at $z = -b_U$ for the governing equation (2a). Because the coefficient $\xi(t)$ depends on $P_0(t)$, (3d) is nonlinear and it is difficult to find the accurate analytical solution of (2a), (2b) and (3d). Replacing $P_0(t)$ by P_{atm}, and $\sum_{i=1}^{N} A_i \cos(\omega_i t + c_i)$ by its temporal mean, i.e., zero, then the right-hand side of (3e) can be simplified into a constant defined as

$$d \stackrel{\text{def.}}{=} 1 + \rho^w g(D - b_U)/P_{atm}. \quad (3f)$$

When $\rho^w g \sum_{i=1}^{N} A_i \ll P_{atm}$ and the variation magnitude of $P_0(t)$ is less than 10% of the atmosphere pressure P_{atm}, d is an adequate approximation of $\xi(t)$. Replacing $\xi(t)$ in the nonlinear boundary condition (3d) by d, yields

$$\left(\frac{\partial P^a}{\partial t} - \frac{k_U \rho^w g}{d \mu^a n_{aL}} \frac{\partial P^a}{\partial z}\right)\Big|_{z=-b_U} = -\frac{\rho^w g}{d} \sum_{i=1}^{N} A_i \omega_i \sin(\omega_i t + c_i). \quad (3g)$$

Equation (3g) is an approximate linearization of equation (3d).

3. Analytical Solution and Numerical Verification

[15] In this section, first the analytical solution of (2a), (2b) and (3g) will be given, then it will be compared with the numerical solutions of the original nonlinear model. The numerical solution is obtained by running TOUGH2 program. The comparison will examine the accuracy of the analytical solution as well as the reasonability and reliability of the assumptions 5–7 on which the analytical solution is based.

3.1. Analytical Solution

[16] On the basis of the superposition principle and the complex transformation used by *Li et al.* [2002], the solution $P^a(z, t)$ to the boundary value problem (2a), (2b) and (3g) can be derived straightforwardly. The details will not be given due to space limitation. For convenience of discussion, two new dimensionless parameters are introduced. They are the upper layer's air-leaking-resistance parameter θ_j [L^{-1}] with respect to the jth sinusoidal component of $H_P(t)$, and the dimensionless parameter r

$$\theta_j = b_U \sqrt{\frac{\omega_j n_{aU} \mu^a}{2 k_U P_{atm}}}, \qquad j = 1, \cdots, N, \quad (4a)$$

$$r = \frac{\rho^w g b_U}{2 P_{atm}} \frac{n_{aU}}{n_{aL}}. \quad (4b)$$

The air-leaking-resistance parameter θ_j describes the magnitude of the leaking resistance of the upper layer to the airflow induced by the jth sinusoidal component of $H_P(t)$. A greater air-leaking-resistance parameter θ_j will lead to greater air pressure in the unsaturated zone in the lower layer. The solution $P^a(z, t)$ can be written as

$$P^a(z,t) = P_{atm} + \rho^w g \sum_{j=1}^{N} A_j \sigma\left(z/b_U; d, r, \theta_j\right) \cdot \cos\left[\omega_j t + \tau\left(z/b_U; d, r, \theta_j\right) + c_j\right], -b_U < z < 0, \quad (5a)$$

where

$$\sigma\left(z/b_U; d, r, \theta_j\right) = \left|C\left(z/b_U; d, r, \theta_j\right)\right|, \qquad j = 1, \cdots, N, \quad (5b)$$

$$\tau\left(z/b_U; d, r, \theta_j\right) = \frac{\pi}{2} + \mathrm{Arg}\left[C\left(z/b_U; d, r, \theta_j\right)\right], \qquad j = 1, \cdots, N. \quad (5c)$$

Here $\mathrm{Arg}[C(z/b_U; d, r, \theta_j)]$ is the argument of the complex function $C(z/b_U; d, r, \theta_j)$ defined as

$$C\left(z/b_U; d, r, \theta_j\right) = \frac{\theta_j \sinh\left[-(1+\mathrm{i})\theta_j z/b_U\right]}{(1+\mathrm{i}) r \cosh\left[(1+\mathrm{i})\theta_j\right] + \mathrm{i} d \theta_j \sinh\left[(1+\mathrm{i})\theta_j\right]}, \quad j = 1, \cdots, N, \quad (5d)$$

where $\mathrm{i} = \sqrt{-1}$.

Table 1. Values of Model Parameters Used in the Numerical Simulation

	Thickness, m	Absolute Permeability k, m^2	Porosity ϕ	Residual Saturation of Water S_{rw}
Upper layer	3.3	$10^{-16} \sim 10^{-12}$	0.3	0.5
Lower layer	4.05	5×10^{-11}	0.3	0.2

3.2. Numerical Verification of the Analytical Solution

[17] The simplified linear mathematical model (2a), (2b) and (3g) are based on assumptions 5–7, on the governing equation linearization, and on the simplification of boundary condition (3d) by replacing $\xi(t)$ with constant d. It is necessary to justify all these assumptions and simplifications via the comparison of the analytical solution (5a) with the numerical solutions of the original nonlinear model. Table 1 lists the model parameters used for the numerical simulation. The numerical solution of the one-dimensional air-water two-phase nonlinear model is obtained using the EOS3 module of TOUGH2 simulator. The two layers are vertically divided into 199 one-dimensional grids. The vertical increments within the domain range from 0.025 m to 0.05 m. The capillary effects are ignored due to assumption 8. The relative permeability of the lower layer is given by the function of *Fatt and Klikoff* [1959].

[18] Two kinds of head $H_P(t)$ were designed for the pressure at the bottom boundary. The first is a single-component sinusoidal, diurnal fluctuation (see Table 2), and the second is a mixture of diurnal and semidiurnal components (see Table 3). The second is used to examine the error induced by the model linearization or the validity of the superposition principle. The distance D in equation (1) is set to be 6.05 m. In Figures 2 and 3 the analytical solution (5a) (curves) and the numerical solution (circles) of the

Table 2. Values of Parameters to Determine the Single-Component Head Fluctuation $H_P(t)$

	Diurnal Component
Amplitude A_1, m	1.0
Angular frequency ω_1, 1/d	$2\pi/1 = 6.2832$
Phase shift c_1, rad	0.0

original nonlinear model are compared at different depths in the unsaturated zone above the water table when the air permeability of the upper layer ranges from 10^{-16} m^2 to 10^{-12} m^2. Figure 2 used the single-component driving force $H_P(t)$ given by Table 2, and Figure 3 used the two-component driving force $H_P(t)$ given by Table 3. One can see that the discrepancy between the analytical and numerical solutions is acceptable, considering the great value range of the air permeability of the upper layer, the strict assumptions 5–7, and the simplifications of the original nonlinear model and boundary condition (3d). The spatial changes of the numerical solutions of air pressure between the water table and the bottom of the upper layer are so small that all the curves for $-5.05\ \text{m} \le z \le -3.3\ \text{m}$ almost coincide with each other, i.e., the assumption 6 is valid for the parameters in Tables 1, 2, and 3. The head fluctuation are also shown in Figures 2 and 3 for comparisons of the phase shift difference between the fluctuations of the head and air pressure.

4. Discussion of the Analytical Solution

[19] The subsurface water-air flow system has seven hydrogeological parameters: n_{aU}, b_U, k_U, D, n_{aL}, b_L and k_L (air permeability of the lower layer). Because of assumptions 6 and 7, the analytical solution is independent of the two parameters b_L and k_L. The other five parameters n_{aU}, b_U, k_U, D and n_{aL} form three independent and dimensionless parameters d, r and θ_j defined by (3f), (4b) and (4a), respectively. The analytical solution is determined by these three parameters. Because of the validity of the superposition principle for the analytical solution, only one single sinusoidal component will be discussed. The parameter θ_j will be replaced by θ hereafter.

[20] It is important to know the rough ranges of the parameters d, r and θ in real subsurface air-water flow systems. Assume that the upper layer is composed of semipermeable materials such as clay, sandy clay, silt, fine sand or pavements of asphalt or concrete, and the lower layer is composed of permeable or very permeable materials such as sand and gravel. According to *Fetter* [1994, Tables 4.4 and 4.6], the usual value ranges of the parameters n_{aU}, k_U and n_{aL} are: $0.02 \le n_{aU} \le 0.35$, $10^{-16}\ \text{m}^2 \le k_U \le 10^{-12}\ \text{m}^2$, $0.1 \le n_{aL} \le 0.19$. For the geometric parameter b_U and D, it is suitable to assume $1\ \text{m} \le b_U \le 10\ \text{m}$, $0.5\ \text{m} \le D - b_U \le 10\ \text{m}$. On the basis of these and $2\pi\ \text{d}^{-1} \le \omega_j \le 4\pi\ \text{d}^{-1}$, $\mu^a = 1.76 \times 10^{-5}$ kg/(ms), $P_{atm} = 101.3$ kPa, $\rho^w = 1000$ kg/m^3 and $g = 9.8$ m/s^2, using (3f), (4b) and (4a), the value ranges of d, r and θ are $1.05 \le d \le 1.97$, $0.0014 \le r \le 1.0$, and $0.08 \le \theta \le 112.4$. As a result, the discussion ranges of the parameters will be within 0.001–1.0 for r and 0.01–100 for θ. The value range of the parameter d is much narrower than the two others. For the sake of the succinctness and convenience, a fixed value of $d = 1.266$, which is determined by the geometric sizes of the air-water system in section 3.2, will be used in the following discussion.

4.1. Air Pressure Fluctuation Within the Unsaturated Zone of the Lower Layer

[21] Using the solution (5a), the air pressure fluctuation relative to the air pressure P_{atm} in the unsaturated zone of the lower layer can be expressed as

$$p_0(t) = P_0(t) - P_{atm} = \rho^w g A \sigma_0 \cos(\omega t + \tau_0 + c), \qquad (6a)$$

in which

$$\sigma_0 = \sigma(-1; d, r, \theta), \qquad \tau_0 = \tau(-1; d, r, \theta) \qquad (6b)$$

and the subscripts of the parameters A, ω and c are cancelled for convenience. So the air pressure fluctuation is determined by the relative amplitude σ_0 and the phase shift τ_0.

[22] When the upper layer becomes less permeable ($\theta \to \infty$), using $\lim_{\theta\to\infty} \coth[(1+i)\theta] = 1$, one can obtain

$$\lim_{\theta\to\infty} \sigma_0 = \lim_{\theta\to\infty} \sigma(-1; d, r, \theta) = 1/d. \qquad (7)$$

Equation (7) means that as the upper layer becomes less permeable, the relative amplitude will tend to its maximum $1/d$.

[23] Figure 4a shows how the relative amplitude σ_0 changes with the dimensionless air-leaking-resistance parameter θ in the unsaturated zone beneath the upper layer ($W(t) < z \le -b_U$) for different values of r when $d = 1.266$. One can see that the relative amplitude increases with θ for fixed values of r. As θ is sufficiently small, the relative amplitude also tends to zero, which means that when the air permeability of the upper layer is sufficiently great or its thickness is sufficiently small, the air pressure fluctuation will become insignificant. As θ becomes sufficiently great, the relative amplitude tends to $1/d \approx 0.79$, as is indicated by equation (7). For any fixed value of θ, the relative amplitude σ_0 decreases with the porosity-related parameter r. According to the definition (4b) of r, for a given upper layer, the parameters b_U and n_{aU} are fixed, the increase of r is equivalent to the decrease of the air-filled porosity n_{aL} of the lower layer. Given the water table fluctuation, the air volume expelled by a rising water table or sucked by a falling one is proportional to the air-filled porosity. Therefore the decrease of the air-filled porosity will lead to the decrease of the volume of air-water exchange and this will reduce the amplitude of the air pressure fluctuation immediately above the water table.

Table 3. Values of Parameters to Determine the Two-Component Head Fluctuation $H_P(t)$

	Amplitude A_j, m	Angular Frequency ω_j, 1/d	Phase Shift c_j, rad
Diurnal component ($j = 1$)	0.4	$2\pi/1 = 6.2832$	0.0
Semidiurnal component ($j = 2$)	0.6	$2\pi/0.5 = 12.5664$	6.0

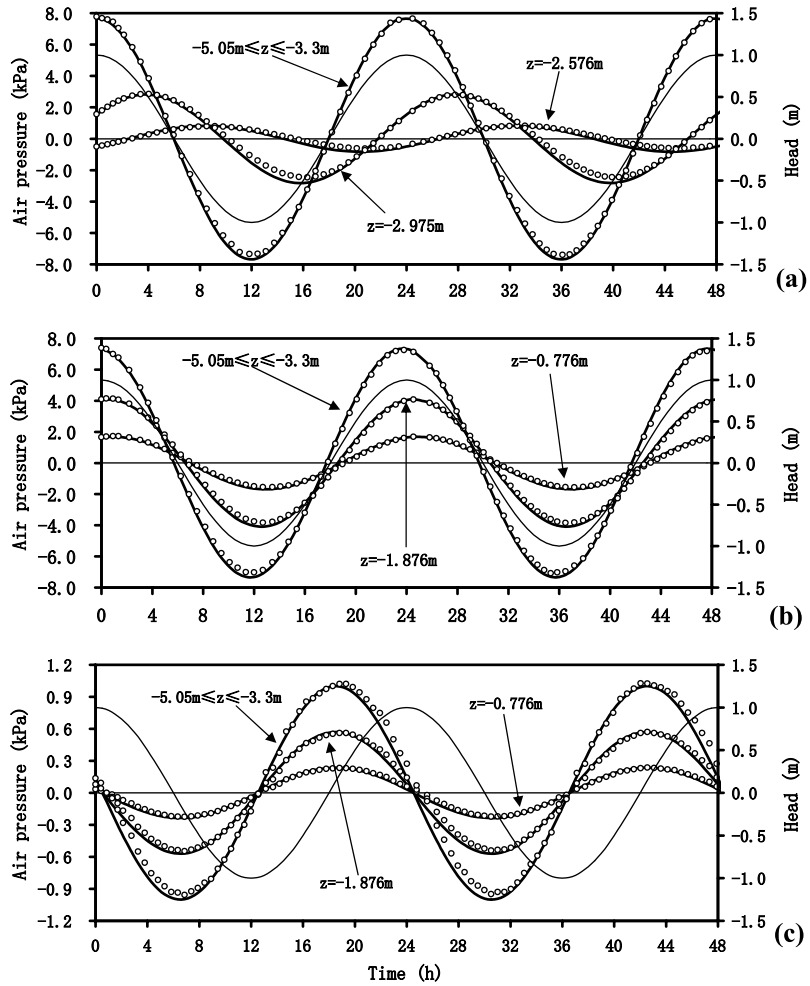

Figure 2. Changes of air pressures with time at different depths in the unsaturated zone above the water table for single-component head $H_P(t)$ given by Table 2 when the air permeability of the upper layer equals (a) 10^{-16} m^2, (b) 10^{-14} m^2, and (c) 10^{-12} m^2. Thick curves, analytical solution (5a); circles, numerical solution to original nonlinear model; thin curves, head $H_P(t)$.

[24] Figure 4b shows how the phase shift τ_0 changes with the dimensionless air-leaking-resistance parameter θ for different values of r when $d = 1.266$. For fixed values of r, the phase shift decreases with θ. As θ is sufficiently small, the phase shift tends to $\pi/2$, which means that when the air permeability of the upper layer is sufficiently great or its thickness is sufficiently small, the air pressure will fluctuate approximately synchronically with the temporal derivative of the head fluctuation. As θ becomes sufficiently great, the phase shift tends to 0. This phenomenon can also be observed in Figure 2a clearly: when $k_U = 10^{-16}$ m^2, the air pressures predicted by both numerical and analytical solutions in the zone $-5.05 < z \leq -3.3$ fluctuate almost synchronically with the head $H_P(t) = A\cos(\omega t + c)$ where $c = 0$. For any $\theta > 0$, Figure 4b shows $0 < \tau_0 < \pi/2$, indicating a "time advance" of the air pressure fluctuation with a value of τ_0/ω compared with the head fluctuation $H_P(t) = A\cos(\omega t + c)$.

4.2. Impact of the Air Pressure on the Water Table

[25] On the basis of pressure balance and assumptions 6–8, the head $H_P(t)$ and the water table $W(t)$ of the unconfined aquifer satisfy equation (3b). Solving equation (3b) for $W(t)$, and substituting equation (6a) into the expression of $W(t)$, yields

$$W(t) = A[\cos(\omega t + c) - \sigma_0 \cos(\omega t + \tau_0 + c)] = A\sigma_w(d, r, \theta)\cos[\omega t + \tau_w(d, r, \theta) + c], \quad (8a)$$

in which σ_w and τ_w are the relative amplitude and phase shift of the sinusoidal fluctuation of the water table $W(t)$, respectively.

[26] Particularly, when the upper layer becomes less permeable ($\theta \to \infty$), one has

$$\lim_{\theta \to \infty} \sigma_w = (d - 1)/d, \quad (8b)$$

which means that as the upper layer becomes less permeable, the amplitude $A\sigma_w$ of the water table fluctuation will approximately only be $(d - 1)/d$ times of that of the head fluctuation. For example, if the upper layer of the two-layered system considered in section (3.2) is clay with an air permeability of $k_U = 10^{-15}$ m^2, and the mean water table is 4.3 m below the ground surface, then one has $d = 1.097$, $r =$

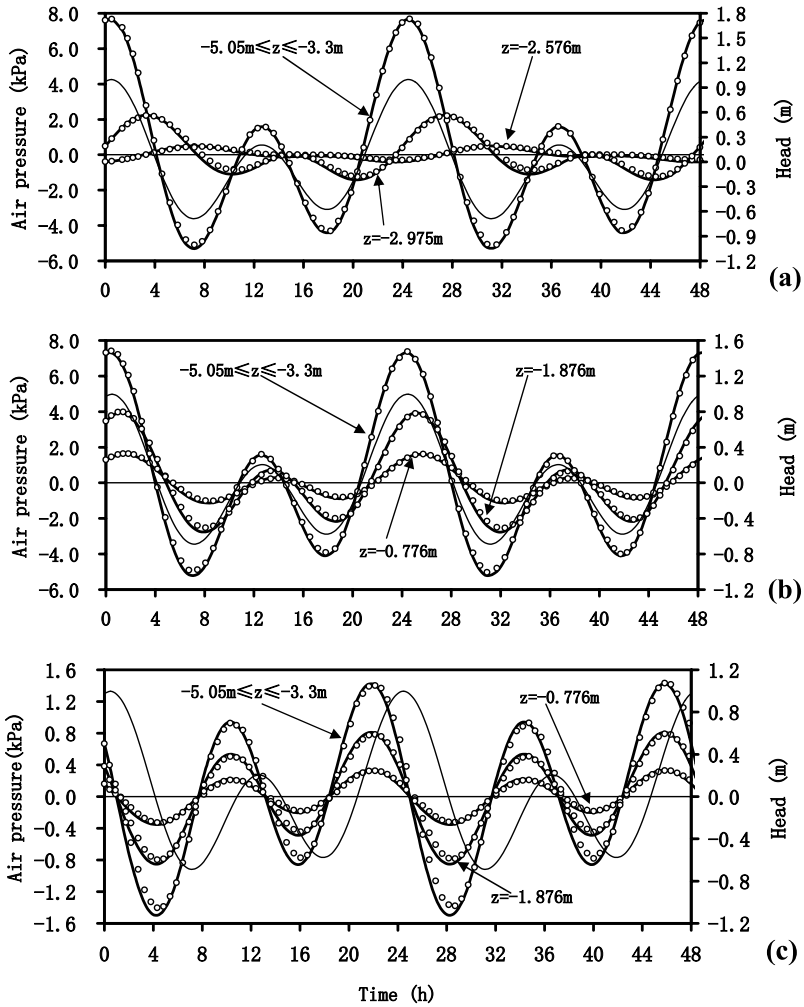

Figure 3. Changes of air pressures with time at different depths in the unsaturated zone above the water table for two-component head $H_P(t)$ given by Table 3 when the air permeability of the upper layer equals (a) 10^{-16} m^2, (b) 10^{-14} m^2, and (c) 10^{-12} m^2. Thick curves, analytical solution (5a); circles, numerical solution to original nonlinear model; thin solid curves, head $H_P(t)$.

0.1, and $\theta = 3.21$ for semidiurnal fluctuation and $\theta = 4.54$ for diurnal fluctuation. Calculation using equation (8a) shows that σ_w equals 11.7% for $\theta = 3.21$ and 10.8% for $\theta = 4.54$. The water table fluctuates with an amplitude which is only about one tenth of that of the head.

[27] It is well known that the landward attenuation of the tide-induced water table fluctuation in a coastal unconfined aquifer is much greater than that in a coastal confined aquifer because the variation of water volume in an unconfined aquifer, which is proportional to the unconfined aquifer's specific yield, is much greater than that of a confined aquifer, which is proportional to the confined aquifer's specific storage. If a coastal unconfined aquifer is covered by a semipermeable layer with great air-leaking resistance, the aquifer becomes "air-confined" and the local water table will fluctuate with an amplitude much less than that of the local head. In this case, although the specific yield of the unconfined aquifer does not change, the variation of water volume in the unconfined aquifer is significantly reduced. Therefore the attenuation of the head fluctuation of this air-confined aquifer will be much slower than that of a common unconfined aquifer where the effects of airflow can be neglected. This is an interesting and important implication for subsurface air-water systems in coastal areas.

4.3. Air Pressure Fluctuation Within the Upper Layer

[28] The air pressure within the upper layer is controlled from top by the constant atmospheric pressure P_{atm} and from below by the spatially uniform air pressure $P_0(t)$. The air pressure fluctuation attenuates upward. Figure 5a shows how the relative amplitude σ of the sinusoidal air pressure fluctuation in the upper layer changes with the dimensionless elevation z/b_U for different values of air-leaking-resistance parameter θ when $d = 1.266$ and $r = 0.1$. The following observations can be made. (1) The relative amplitude $\sigma(z/b_U; d, r, \theta)$ decreases with the elevation. The greater the air-leaking resistance is, the fast the amplitude decreases. (2) For small values of θ (<1) the relative amplitude $\sigma(z/b_U; d, r, \theta)$ linearly decreases from $\sigma_0 = \sigma(-1; d, r, \theta)$ at the bottom of the upper layer to zero at the ground surface.

[29] Figure 5b shows how the phase shift τ of sinusoidal air pressure fluctuation changes with the dimensionless

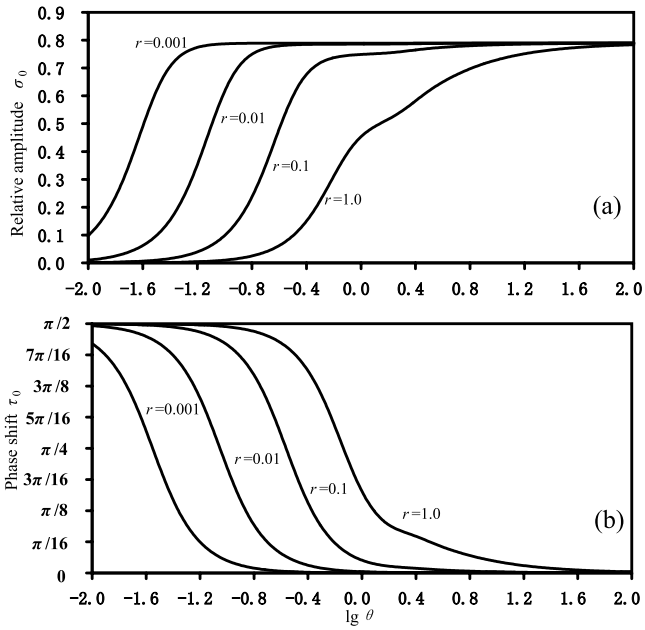

Figure 4. Changes of (a) relative amplitude σ_0 and (b) phase shift τ_0 of sinusoidal air pressure fluctuation at the bottom of the upper layer ($z = -b_U$) with the air-leaking-resistance parameter θ for different values of r when $d = 1.266$.

elevation z/b_U for different values of θ when $d = 1.266$ and $r = 0.1$. In Figure 5b the phase shift $\tau(z/b_U; d, r, \theta) = \pi/2 + \mathrm{Arg}[C(z/b_U; d, r, \theta)]$ is modified to be continuous with respect to z/b_U. The difference between the values of the modified and original phase shifts equals $2n\pi$ at a given elevation z/b_U, where n is an integer dependent on z/b_U. Figure 5b shows that the phase shift $\tau(z/b_U; d, r, \theta)$ approximately remains a constant for small values of θ(<0.6). For large values of θ, as the elevation increases from the bottom of the upper layer to the ground surface, the phase shift first decreases linearly with the elevation, then its decreasing rate tends to zero when the elevation approaches the ground surface due to the atmospheric boundary condition.

5. Application: Case Study at Hong Kong International Airport

[30] The analytical solution (5a) will be used to estimate the air permeability of the marine sand fill material at a coastal area in Hong Kong. The study area was formed from land reclamation (see Figure 6). This area has a three-layered structure. The upper layer mainly comprises 3.3 m thick semipermeable marine sand fill. The middle layer comprises 4 m thick permeable fine rock fill and the lower layer is very permeable coarse rock fill. The middle and lower layer form a very permeable aquifer. The landward vertical cross section is a rectangle 118 m long and 16.3 m high. The left boundary is the water-land interface. The mean sea level is 6.05 m below the ground surface. The maximum amplitude of the sea tide is 1.25 m. The water table fluctuates within fine rock fill of the middle layer. A piezometer in the coarse rock fill about 300 m from the coast shows that the water table fluctuation is almost coincident with that of sea level [*Plant et al.*, 1998]. This suggests that the water table variation in the rock fill layer can be assumed to be identical to the fluctuation of the sea tide [*Jiao and Li*, 2004]. According to the numerical simulations by *Jiao and Li* [2004], the tide-induced airflow in the marine sand can be approximately regarded as vertical at the locations far from left and right boundaries. Therefore the analytical solution can be used to estimate the air permeability of the marine sand fill.

[31] Figure 7a shows the observed and fitted tidal level during the 6-day period from 8 to 13 December 1999. The fitted tidal level equals the sum of diurnal and semidiurnal components given by equation (1), where $D = 6.05$ m, $N = 2$, $A_1 = 0.61$ m, $A_2 = 0.47$ m, $\omega_1 = 0.26\ \mathrm{h}^{-1}$, $\omega_2 = 0.51\ \mathrm{h}^{-1}$, $c_1 = 1.03$, $c_2 = 0.93$. From the beginning of December 1999 to the end of February 2000, significant air pressure fluctuation was observed from a vibrating wire piezometer CP327 installed at the elevation about 3.05 m below the ground surface (see Figure 6). Unfortunately, the detailed data are not available to the authors. From a curve of time versus air

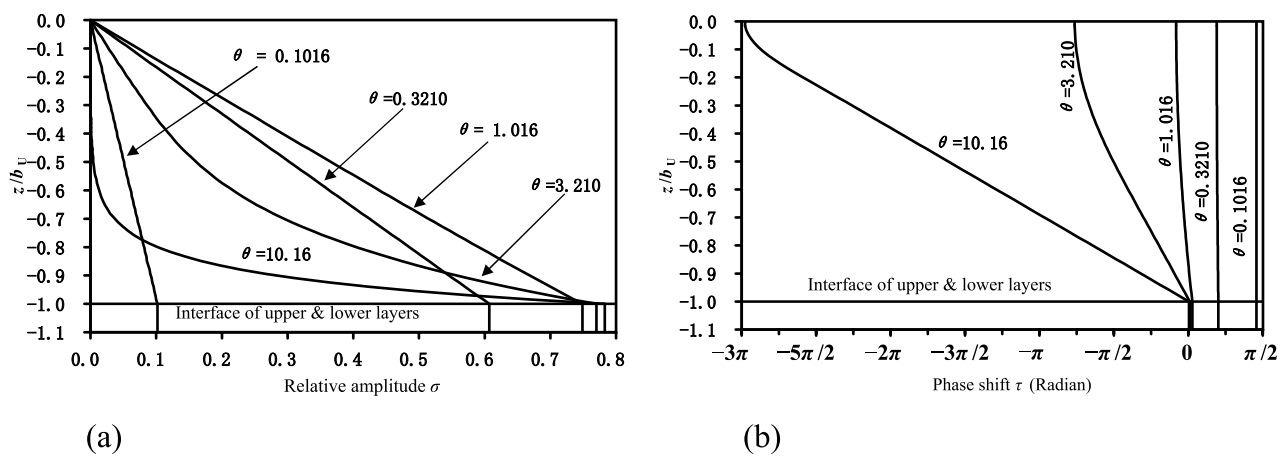

Figure 5. Changes of (a) relative amplitude σ and (b) phase shift τ of sinusoidal air pressure fluctuation in the upper layer with the dimensionless elevation z/b_U for different values of air-leaking-resistance parameter θ when $d = 1.266$ and $r = 0.1$.

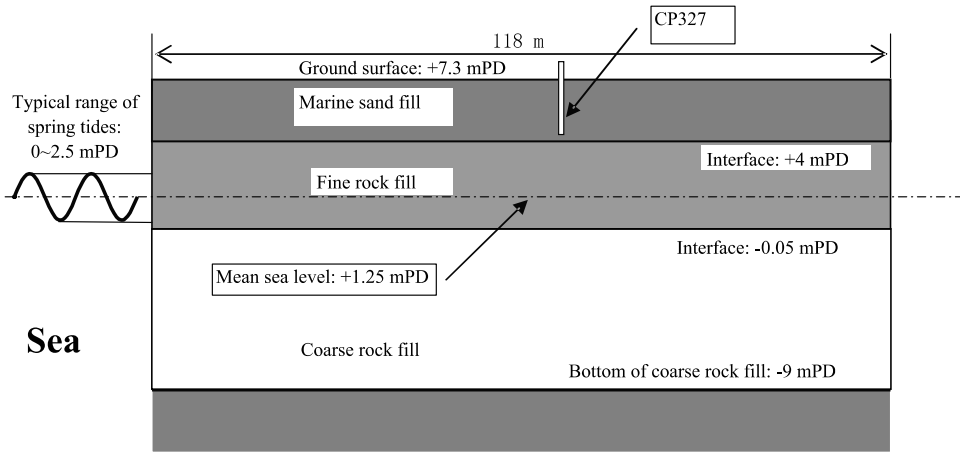

Figure 6. Cross section of a coastal reclamation area in Hong Kong.

pressure during the 90-day period calibrated against the atmospheric pressure, the difference of the daily maximum and minimum air pressures can be read to range from 1.2 kPa to 2.1 kPa. These data will be used to determine the value range of the air permeability of the marine sand layer based on the analytical solution.

[32] The air pressure changes with time at 3.05 m below the ground surface was calculated using the analytical solution (5a) and the fitted water table fluctuation $H_P(t)$ shown as the solid curve in Figure 7a. The results are shown in Figure 7b. In the calculation, the porosities of the marine sand layer and fine rock layer are fixed to be $n_{aU} = 0.3 \times 0.5 = 0.15$, $n_{aL} = 0.3 \times 0.8 = 0.24$, which are the same as those of *Jiao and Li* [2004]. One can see that when k_U increases from 1.2×10^{-12} m^2 to 2.0×10^{-12} m^2, the difference of the daily maximum and minimum air pressures in the 6-day period decreases from 2.1 kPa to 1.2 kPa. Therefore the value range of the air permeability is 1.2×10^{-12} m^2 $\leq k_U \leq 2.0 \times 10^{-12}$ m^2.

6. Conclusions

[33] This paper investigates the vertical airflow driven by periodically fluctuating water table within a permeable layer overlain by a semipermeable, unsaturated layer. The water table fluctuation induces breathing of the upper layer and air pressure fluctuation in the unsaturated zone. An analytical solution of the air pressure fluctuation is derived based on some assumptions and model linearization approximations, the reasonability and reliability of which were investigated by comparison of the analytical solution with the numerical solution of the original nonlinear model of air-water two-phase flow.

[34] Because of the significant air pressure fluctuation beneath the upper layer, the water table $W(t)$ will differ significantly from the head $H_P(t)$. For a sinusoidal head $H_P(t)$, the upper layer's impacts on the air pressure fluctuation can be mainly characterized by the air-leaking-resistance parameter θ. In the unsaturated zone beneath the upper layer, the air pressure fluctuates with an advanced phase shift less than $\pi/2$ and greater than 0. The amplitude of the air pressure fluctuation increases with θ. For small θ the phase shift approximates $\pi/2$ and the air pressure is approximately proportional to the temporal derivative of $H_P(t)$. This conclusion is similar to that of the numerical modeling by *Jiao and Li* [2004]. For sufficiently great θ the phase shift approximates 0 and the air pressure is approximately proportional to the head $H_P(t)$. The water table fluctuation amplitude, which decreases with θ, is always less than that of the piezometer head $H_P(t)$ and can only be approximately one tenth of the latter for a two-layered system with typical parameter values if $\theta > 3$, which can be satisfied by a clay layer with an air permeability of $k_U = 10^{-15}$ m^2 and thickness of a few meters. If a coastal unconfined aquifer is covered by a layer with great air-

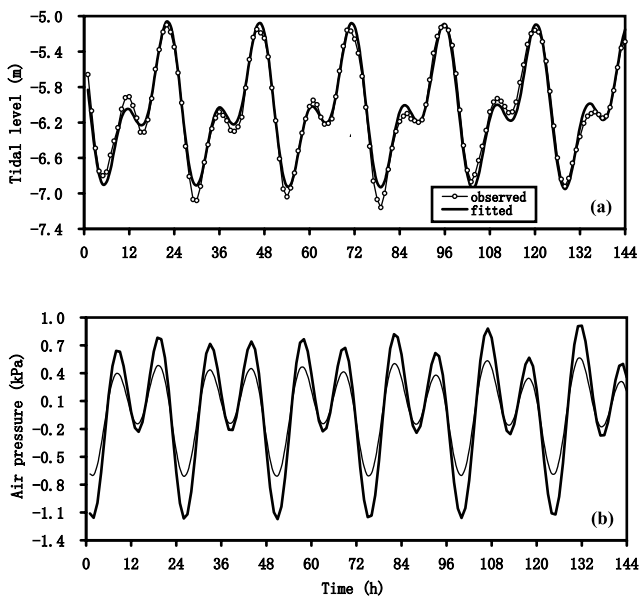

Figure 7. (a) Observed (curve with circles) and fitted (solid curve) water table fluctuation during the 6-day period from 8 to 13 December 1999 and (b) predicted changes of the air pressure with time in the same period at 3.05 m below the ground surface when the air permeability of the marine sand fill equals 1.2×10^{-12} m^2 (thick curve) and 2×10^{-12} m^2 (thin curve). The prediction is based on the analytical solution (5a) and the fitted water table fluctuation shown as the solid curve in Figure 7a.

leaking resistance such as clay or asphalt pavement, the landward attenuation of the tide-induced head fluctuation of this air-confined aquifer will be much slower than that of a common unconfined aquifer where the effect of the airflow on the water table is negligible.

[35] In the upper layer, the amplitude of the air pressure fluctuation reaches the maximum at its bottom and equals zero at the ground surface. The amplitude decreases with the elevation. The greater the air-leaking resistance is, the greater the decreasing rate of the amplitude with respect to the elevation. If the air-leaking resistance is less than 0.6, the amplitude decreases linearly with the elevation and the phase shift is approximately independent of the elevation.

[36] The lower layer's impact on the air pressure fluctuation can be mainly characterized by the air-filled porosity of the lower layer, and the distance between the mean water table and the roof of the lower layer. The relative amplitude of the air pressure (ratio of the amplitude to $\rho^w gA$) is bounded by $1/d$, and the ratio of amplitude of the water table fluctuation to that of the head $H_P(t)$ is bounded by $(d-1)/d$.

[37] The analytical solution was used to estimate the air permeability of the marine sand fill at a coastal, reclamation area of Hong Kong based on the diurnal and semidiurnal fitting to the observed tidal level fluctuations and amplitudes of air pressure fluctuation. The air permeability of the marine sand fill is between 1.2×10^{-12} m^2 and 2.0×10^{-12} m^2.

[38] **Acknowledgment.** This research was supported by the National Natural Science Foundation of China (40372111) and the Hong Kong Research Grants Council (RGC) of the Hong Kong Special Administration Region, China.

References

Baehr, A. L., and M. F. Hult (1991), Evaluation of unsaturated zone air permeability through pneumatic tests, *Water Resour. Res.*, *27*, 2605–2617.

Elberling, B., F. Larsen, S. Christensen, and D. Postma (1998), Gas transport in a confined unsaturated zone during atmospheric pressure cycles, *Water Resour. Res.*, *34*, 2855–2862.

Fatt, I., and W. A. Klikoff (1959), Effect of fractional wettability on multiphase flow through porous media, *Trans. Am. Inst. Min. Metall. Pet. Eng.*, *216*, 246–251.

Fetter, C. W. (1994), *Applied Hydrogelogy*, Prentice-Hall, Upper Saddle River, N. J.

GCG (Asia) (2001), Summary of GCG Heave Investigation, *Rep. R31/6*, Hong Kong, China.

Illman, W. A., and S. P. Neuman (2000), Type-curve interpretation of multirate single-hole pneumatic injection tests in unsaturated fractured rock, *Ground Water*, *38*, 899–911.

Illman, W. A., and S. P. Neuman (2001), Type-curve interpretation of a cross-hole pneumatic injection test in unsaturated fractured tuff, *Water Resour. Res.*, *37*, 583–603.

Jiao, J. J., and H. Li (2004), Breathing of coastal vadose zone induced by sea level fluctuations, *Geophys. Res. Lett.*, *31*, L11502, doi:10.1029/2004GL019572.

Massmann, J. W. (1989), Applying groundwater flow models in vapor extraction system design, *J. Environ. Eng.*, *115*(1), 129–149.

McWhorter, D. B. (1990), Unsteady radial flow of gas in the vadose zone, *J. Contam. Hydrol.*, *5*, 297–314.

Li, H., and J. J. Jiao (2003), Influence of the tide on the mean watertable in an unconfined, anisotropic, inhomogeneous coastal aquifer, *Adv. Water Resour.*, *26*, 9–16.

Li, H., J. J. Jiao, M. Luk, and K. Cheung (2002), Tide-induced groundwater level fluctuation in coastal aquifers bounded by an L-shaped coastline, *Water Resour. Res.*, *38*(3), 1024, doi:10.1029/2001WR000556.

Li, H., J. J. Jiao, and M. Luk (2004), A falling-pressure method for measuring air permeability of asphalt in laboratory, *J. Hydrol.*, *286*, 69–77.

Li, L., and D. A. Barry (2000), Wave-induced beach groundwater flow, *Adv. Water Resour.*, *23*, 325–337.

Moridis, G. J., and K. Pruess (1995), Air barriers for waste containment in the subsurface, paper presented at the 1995 TOUGH Workshop, Lawrence Berkeley Lab., Berkeley, Calif., 20–22 March.

Nielsen, P. (1990), Tidal dynamics of the water table in beaches, *Water Resour. Res.*, *26*, 2127–2134.

Nielsen, P., and P. Perrochet (2000), Watertable dynamics under capillary fringes: Experiments and modeling, *Adv. Water Resour.*, *23*, 503–515.

Plant, G. W., C. S. Covil, and R. A. Hughes (1998), *Site Preparation for the New Hong Kong International Airport: Design, Construction and Performance of the Airport Platform*, Thomas Telford, London.

Pruess, K., C. Oldenburg, and G. Moridis (1999), TOUGH2 user's guide, version 2.0, Lawrence Berkeley Natl. Lab., Univ. of California, Berkeley, Berkeley, Calif.

Ross, B., and N. Lu (1994), Efficiency of air inlet wells in vapor extraction systems, *Water Resour. Res.*, *30*, 581–584.

Shan, C. (1995), Analytical solutions for determining vertical air permeability in unsaturated soils, *Water Resour. Res.*, *31*, 2193–2200.

Shan, C., R. W. Falta, and I. Javandel (1992), Analytical solutions for steady state gas flow to a soil vapor extraction well, *Water Resour. Res.*, *28*, 1105–1120.

Shan, C., I. Javandel, and P. A. Witherspoon (1999), Characterization of leaky faults: Study of air flow in faulted vadose zones, *Water Resour. Res.*, *35*, 2007–2013.

Stonestrom, D. A., and J. Rubin (1989), Air permeability and trapped-air content in two soils, *Water Resour. Res.*, *25*(9), 1959–1969.

Weir, G. J., and W. M. Kissling (1992), The influence of airflow on the vertical infiltration of water into soil, *Water Resour. Res.*, *28*, 2765–2772.

J. J. Jiao, Department of Earth Sciences, University of Hong Kong, Hong Kong, China. (jjiao@hku.hk)

H. Li, Department of Mathematics, Anshan Normal University, Anshan 114005, China. (hailong@graduate.hku.hk)